Preprints of the 20th World Congress
The International Federation of Automatic Control
Toulouse, France, July 9-14, 2017

Inverse Optimal Impulsive Control Based Treatment of Influenza Infection ⋆

Gustavo Hernandez-Mejia * **Alma Y. Alanis** *
Esteban A. Hernandez-Vargas **

* *CUCEI, Universidad de Guadalajara, C.P.44430,Guadalajara, Mexico (almayalanis@gmail.com, gustavohdezm@gmail.com)*
** *Frankfurt Institute for Advanced Studies, Ruth-Moufang-Strasse 1, 60438, Frankfurt am Main, Germany (vargas@fias.uni-frankfurt.de)*

Abstract: Seasonal and pandemic influenza A virus (IAV) infections are a cause of severe morbidity and mortality worldwide. In this work, we study the problem of influenza treatment from a control theory perspective. Combined techniques of impulsive control and inverse optimal control are applied to an IAV model. Numerical results show that control-based strategies could improve virological efficacy and at the same time may reduce the drug amount in comparison to current clinical recommendations of pandemic regimens. This work discusses the advantages of theoretical approaches to tackle influenza infections.

Keywords: Influenza A Virus, PK/PD Dynamics, Inverse Optimal Control, Impulsive Control.

1. INTRODUCTION

Seasonal influenza is an acute viral infection that can spread fast from person to person, causing annual epidemics and outbreaks. Annual epidemics are estimated to result in about 3 to 5 million cases of severe illness and about 250000 to 500000 deaths [WHO (2014)]. Antiviral drugs and influenza vaccines play a key role in prevention and treatment of acute IAV infections. The most commonly used Food and Drug Administration (FDA) approved antiviral drugs are neuraminidase inhibitors, among the most important are Zanamivir, Peramivir, and Oseltamivir. These can reduce the severity and duration of influenza symptoms and associated complications [Gubareva et al. (2000)].

Therapy efficacy can be evaluated under two principal indicators, the virological efficacy index and the total amount of drug [Canini et al. (2014)]. The first indicates the efficacy of the drug clearing the virus, the second reports the quantity of drug administrated. Nowadays pharmaceutical companies consider a strategic initiative to implement modeling approaches within drug projects. To this end, the Pharmacokinetics (PK) and Pharmacodynamics (PD) modelling and simulation provide a framework for linking interactions between drugs, pharmacological targets, physiological pathways and integrated disease systems [Agoram et al. (2007),Van der Graaf and Benson (2011)].

Influenza treatment recommendation is formed by fixed doses of drug at fixed time intervals [WHO (2009)]. Several diseases have been analysed from an engineering approach like HIV [Hernandez-Vargas et al. (2011), Chang et al. (2012) Rivadeneira et al. (2014), Hernandez-Vargas et al. (2014), Rocha et al. (2016)], Diabetes [Leon et al. (2013), Chandgude and Pawar (2016)] or epidemiological level [Bakare et al. (2014)], improving treatments and recovering from illness. Among different infectious diseases, several theoretical works have been developed to control HIV infection and to mitigate viral mutation [Rivadeneira and Moog (2012), Hernandez-Vargas et al. (2013)].

In [Lee et al. (2013), Jaberi-Douraki and Moghadas (2014), Imran et al. (2016)] authors addressed influenza treatments to an epidemiological level to reduce transmission between hosts, however, control-based strategies remain largely unexplored at the host level. Here, we consider that antiviral therapies can be tailored to measurements of CD8+ T cells and the influenza A virus (IAV), aiming to have the highest virological efficacy.

The paper is organized as follows: Section 2 describes the IAV and PK/PD dynamics model including parameters. In Section 3, theoretical concepts of the inverse optimal impulsive control are introduced. Subsection 3.1 shows the integration of the IAV model and impulsive control to estimate the drug dose. Subsection 3.2 indicates performance indices to evaluate drug treatments. To test the performance of the proposed methodology, Section 4 presents a comparison of the control-based strategy and the common treatment recommendations by the FDA [FDA (2008)]. Section 5 presents conclusions and future research.

2. MODELLING FRAMEWORK

In the last years, novel modelling and simulation contributions have been developed in IAV infection dynamics [Boianelli et al. (2015)]. Here, we consider the model proposed by Boianelli *et al.*, which consists on the virus (V) and CD8+ T cells (E) dynamics at a host level. Parameter values, estimation procedures and identifiability studies

⋆ This work was supported by CONACyT-Mexico through the project CB256769, DAAD Germany through the program PROALMEX funding the project OPTREAT, and by the Alfons und Gertrud Kassel-Stiftung.

are reported in [Boianelli et al. (2015)]. The IAV model is formed with the following equations:

$$\dot{E} = S_E + rE\left(\frac{V}{V+k_e}\right) - c_e E \tag{1}$$

$$\dot{V} = pV\left(1 - \frac{V}{k_v}\right) - c_v V E. \tag{2}$$

The CD8+ T cells homeostatic replenishment rate is $S_E = c_e E(0)$, where c_e is the half life of CD8+ T cells and $E(0)$ is the initial number of these cells. E cells proliferation promoted by the virus follows a logistic growth with half saturation constant k_e. In this model, the virus replicates with a logistic function, with a maximum carrying capacity k_v and the replication rate p. The virus is cleared with rate $c_v E$. A graphical description of the model is presented in Fig. 1 and model parameters are shown in Table 1.

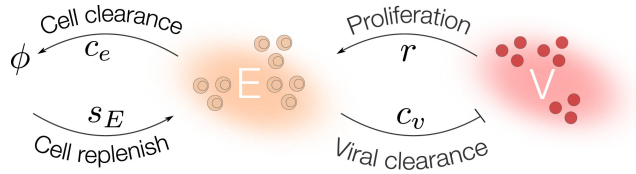

Fig. 1. The IAV virus (V) promotes CD8+ T cells (E) proliferation with a rate r. Viral clearance rate is determined by c_v.

Table 1. IAV model parameters.

Parameter	Nominal value	Units
r	0.33	days^{-1}
k_e	2.7×10^3	PFU/mL
c_e	2.0×10^{-2}	days^{-1}
S_E	2.0×10^4	$\text{days}^{-1}\text{cells}$
p	4.4	days^{-1}
k_v	10^6	PFU/mL
c_v	1.24×10^{-6}	$\text{days}^{-1}\text{cells}^{-1}$
$E(0)$	10^6	cells
$V(0)$	25	PFU/mL

2.1 PK/PD Modelling

Antiviral PK/PD dynamics are needed to study the effect of drugs on influenza infections. The PK phase describes the temporal distribution of drug concentration in different organs. This can be modeled by a constant decay differential equation $\dot{D} = -\delta_D D$ where D is the amount of drug available and δ_D is the drug elimination rate. On the other hand, the PD phase describes the effect of a drug on the organism. PD dynamics can be represented by $\eta = \frac{D}{D+EC_{50}}$ indicating the efficacy of the treatment, where the parameter EC_{50} is the drug concentration level at which provides the 50% of drug efficacy.

Drug intake time is defined by τ_k, where $\{k = 1, 2, \cdots\}$ indicates the sequence of drug intakes. In order to link the antiviral therapy with the IAV model, we consider that the viral replication rate p can be replaced by $p(1-\eta)$, based on the fact that antiviral therapies mainly affect the replication cycle of the virus. Consequently, the equation (2) can be rewritten as

$$\dot{V} = p\left(1 - \frac{D}{D+EC_{50}}\right)V\left(1 - \frac{V}{k_v}\right) - c_v V E \tag{3}$$

with

$$\dot{D}(t) = -\delta_D D(t),\ \tau_k \leq t < \tau_{k+1} \tag{4}$$

with $\tau_k \leq t < \tau_{k+1}$ the time intervals between drug intakes. This indicates that the first drug intake of the treatment is given by $D(\tau_1) = D(t_0)$. In this way, PK/PD and IAV model are integrated. PK/PD parameters are listed in Table 2.

Table 2. Oseltamivir PK/PD parameters [Wattanagoon et al. (2009), WHO (2009), FDA (2008)]

Parameter	Nominal value	Units
EC_{50}	42.30	mg
δ_D	3.26	days^{-1}
$\tau_{k+1} - \tau_k$	0.5	days

3. INVERSE OPTIMAL IMPULSIVE CONTROL

Given a plant P whose state variables are denoted by $X \in \Re^n$, a set of *control instants* $T = \{\tau_k\}$, $\tau_k \in \Re$, $\tau_k < \tau_{k+1}$, $k = 1, 2, \cdots$, and *control laws* $U(k, X) \in \Re^n$, $k = 1, 2, \cdots$. At each τ_k, X is changed impulsively by $X(\tau_k^+) = X(\tau_k^-) + U(k, X)$ such that the output $Y = f(X)$, $f : \Re^n \to \Re^m$ approaches the goal $Y^* \in \Re^m$ as $k \to \infty$ [Yang (1999)].
Impulsive control system dynamics are governed by its Ordinary Differential Equations (ODEs) when $t \neq \tau_k$, so whenever $t \neq \tau_k$, the controlled system is at open loop (free system). Only at the instant τ_k, $k = 1, 2, \cdots$, and considering an impulsive control state space system $\Delta X\,|_{t=\tau_k} = By$, the state variable is instantaneously changed from $X(\tau_k^-)$ to $X(\tau_k^+) = X(\tau_k^-) + U(k, X) = X(\tau_k^-) + By$.

Given $y = Cx$, $y \in \Re^m$ is the output, the impulsive control system can be written as

$$\begin{aligned} \dot{x} &= Ax + \phi(x),\ t \neq \tau_k \\ \Delta X\,|_{t=\tau_k} &= BCx,\ k = 1, 2, \cdots \\ x(t_0^+) &= x_0 \end{aligned} \tag{5}$$

where $\phi : \Re^n \to \Re^n$ is a nonlinear function, $x \in \Re^n$, A is a $n \times n$ constant matrix, B is a $n \times m$ constant matrix and C is a $m \times n$ constant matrix, one can see that $U(k, X) = BCx$, further details can be found in Yang (1999).

Haddad [Haddad et al. (2006)] proposed a strategy for the *inverse optimal hybrid control problem* parameterizing a family of stabilizing hybrid controllers. This minimizes a *derived* cost functional that provides flexibility in the specific control law. Consider the non-linear impulsive controlled system

$$\dot{x}(t) = f_c(x(t)) + G_c(x(t))u_c(t),\ t \neq \tau_k \tag{6}$$

$$\Delta x(t) = f_d(x(t)) + G_d(x(t))u_d(t),\ t = \tau_k \tag{7}$$

with $x(0) = x_0$, $k = 1, 2, \cdots$, and performance functional

$$J(x_0, u_c(\cdot), u_d(\cdot)) = \int_0^\infty \{J_1(x(t)) + J_2(x(t), t)\}\, dt + \sum_{k \in \mathbb{Z}_{[0,\infty)}} \{J_3(x(t_k)) + J_4(x(t_k), t_k)\} \quad (8)$$

where

$$J_1(x(t)) = L_{1c}(x(t))$$
$$J_2(x(t), t) = u_c^T(t) R_{2c}(x(t)) u_c(t)$$
$$J_3(x(t_k)) = L_{1d}(x(t_k))$$
$$J_4(x(t_k), t_k) = u_d^T(t_k) R_{2d}(x(t_k)) u_d(t_k)$$

with $(u_c(\cdot), u_d(\cdot))$ is an *admissible hybrid control*. Assume there exist a continuously differentiable function $W : \Re^n \to \Re$, and functions $P_{12} : Z_{\tau_k} \to \Re^{1\times m_d}$, $P_2 : Z_{\tau_k} \to N^{m_d}$ such that $W(0) = 0$, $W(x) > 0$, $x \in \Re^n$, $x \neq 0$. $L_{1c} : \Re^n \to \Re$ and satisfies $L_{1c}(x) \geqslant 0$, $R_{2c} : \Re^n \to P^{m_c}$. $L_{1d} : Z_{\tau_k} \to \Re$ and satisfies $L_{1d}(x) \geqslant 0$, $R_{2d} : Z_{\tau_k} \to P^{m_d}$. Also, $f_c : M \to R^n$, $f_d : S \to R^n$. M is an open set with $0 \in M$, and $S \subset [0, \infty) \times M$ is the resetting set, $x(t) \in M \subseteq \Re^n$. P^{m_c} and P^{m_d} are positive definite matrices with size $m_c \times m_c$ and $m_d \times m_d$, respectively, N^{m_d} is a $m_d \times m_d$ nonnegative definite matrix.

The zero solution for the closed-loop system in (6) and (7) is globally asymptotically stable with the *hybrid feedback control law*

$$u_c(t) = \phi_c(x) = -\frac{1}{2} R_{2c}^{-1}(x) G_c^T(x) W'^T(x),\ t \neq \tau_k \quad (9)$$
$$u_d(t) = \phi_d(x) = -\frac{1}{2}(R_{2d}(x) + P_2(x))^{-1} P_{12}^T(x),\ t = \tau_k \quad (10)$$

and the performance functional (8), with

$$L_{1c}(x) = \phi_c^T(x) R_{2c}(x) \phi_c(x) - W'(x) f_c(x), \quad (11)$$
$$L_{1d}(x) = \phi_d^T(x)(R_{2d}(x) + P_2(x))\phi_d(x) - W(x + f_d(x)) + W(x), \quad (12)$$

which is minimized in the sense that

$$J(x_0, \phi_c(x(\cdot)), \phi_d(x(\cdot))) = \min_{\xi} J(x_0, u_c(\cdot), u_d(\cdot)),$$
$$x_0 \in \Re^n, \xi = (u_c(\cdot), u_d(\cdot)) \in \Omega(x_0) \quad (13)$$
$$J(x_0, \phi_c(x(\cdot)), \phi_d(x(\cdot))) = W(x_0),\ x_0 \in \Re^n. \quad (14)$$

Here, $\Omega(x_0)$=$(u_c(\cdot), u_d(\cdot))$ is admissible and $x(\cdot)$ given by (6) and (7) satisfies that $x(0) \to 0$ as $t \to \infty$. The formal proof and further explanations can be found in [Haddad et al. (2006)].

3.1 Control-Based Drug Estimation

The closed-loop IAV-PK/PD model in (1), (3) and (4) can be represented as the impulsive controlled system in (6) and (7), with the drug state variable D impulsively changed as in (5) and control law (10). The closed-loop system representation is as follow

$$f_c(x(t)) = \begin{cases} p\left(1 - \dfrac{D}{D + EC_{50}}\right) V \left(1 - \dfrac{V}{k_v}\right) - c_v V E \\ -\delta_D D \end{cases} \quad (15)$$

$$x \triangleq [V, D]^T$$
$$\Delta x = \Delta D(\tau_k) = f_d(x(t)) + \phi_d(x(t)) \quad (16)$$
$$f_d(x(t)) = -\delta_D D$$
$$\phi_d(x(t)) = abs\left(-\frac{1}{2}(R_{2d}(x) + P_2(x))^{-1} P_{12}^T(x)\right)$$

the equation (15) performs in $t \neq \tau_k$ and (16) in $t = \tau_k$, *abs* in $\phi_d(x(t))$ denotes the absolute value $|\cdot|$. This restriction is considered due to only positive drug amounts can be provided.

Notice that due to treatment properties of the combined IAV-PK/PD model, the second term in (6) does not represent any control law and $u_c(t) = \phi_c(x) = 0$, $t \neq \tau_k$ in (15). This means that there is no drug intake between k-esimes control instants, letting (9) equal to zero. In addition, in (16) $\phi_d(x(t))$ drives the control action and changes impulsively the drug state D. In this sense, $\Delta D(\tau_k) = D(\tau_k^-) + \phi_d(x(t)) = D(\tau_k^+)$ moves the initial condition of D, before every free system period as in (5). This determines the control-based amount of drug necessary to inhibit viral replication.

3.2 Treatment Strategies and Performance Indices

We consider different treatment strategies. First, we study the IAV model (1), (3) and (4) without drug treatment. Second, we test the effects with drug influence by FDA treatment recommendations, that is periodic fixed doses, $\Delta D(\tau_k) = D_{fixed}$ on each intake. Note that the World Health Organization (WHO) suggests two treatment levels, curative regimen with $D_{fixed} = 75$ mg and a pandemic regimen $D_{fixed} = 150$ mg [WHO (2009)].

Following (15) and (16) with the first instant $D(\tau_1) = 75$ mg for curative or $D(\tau_1) = 150$ mg for pandemic regimen, we evaluate the effects of the control-based treatment with two levels of drug concentration as initial dose and different treatment initiation, these are days 2, 3 and 4 post influenza challenge ($t_0 = 2, 3, 4$). The treatment is active until day 10. The virological efficacy index Ψ is defined as

$$\Psi = 100\left(1 - \frac{AUC_c}{AUC}\right)\% \quad (17)$$

where AUC_c represents the area under the dynamics of V with treatment and AUC is the area under the curve of V without treatment [Canini et al. (2014), Boianelli et al. (2016)]. It is important to remark that these areas are calculated from time zero until the time when the viral load is less than 50 copies per mL. On the other hand, the total amount of drug is the sum of doses from the first intake until 10 days post infection.

4. RESULTS

Results of the different treatments strategies are numerically computed using Matlab. Expressions (15) and (16) are programmed in such a way the initial intake time t_0 can be modified for different tests and the control-based drug dose is calculated by these equations.

The model is solved until the first drug intake, then for a control instant, the program calculates the amount of drug that is applied to the system. The process is repeated until simulation time ends, here we use 10 days of simulation time. Note that control parameters in (16) need to be defined by the user. In this paper, control parameters were fine-tuned as follows:

$$R_{2d} = \begin{pmatrix} 120 & 0 \\ 0 & 5 \end{pmatrix}, P_2 = \begin{pmatrix} 14 & 0 \\ 0 & 1 \end{pmatrix} \quad (18)$$
$$P_{12} = (1000000 \;\; 1000), G_d = 1.7$$

We consider that the matrix P_2 is modified by the drug. R_{2d} and P_{12} are assumed to be affected by IAV dynamics. These values are obtained heuristically based on the impact of the virus. G_d is a constant control gain.

4.1 Treatment Strategies Comparison

Simulation results in Fig. 2 show the virus, CD8+ T cells, and drug dynamics. The evolution of the virus and CD8+ T cells without treatment is also plotted. The drug dynamics shows fixed doses for the therapy proposed by the FDA while control-based therapy shows different doses for each intake time.

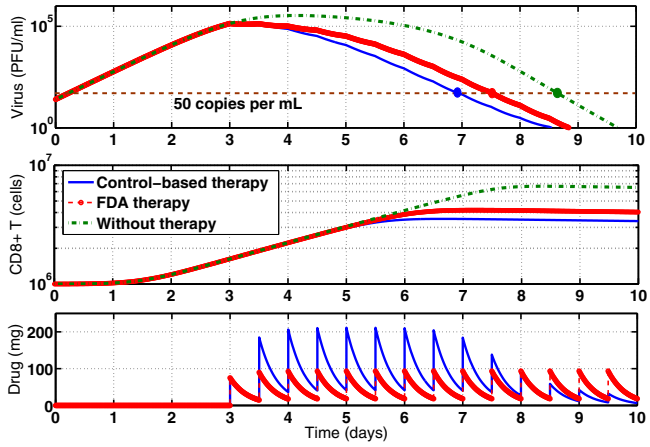

Fig. 2. Treatment strategies initiating at day 3. Curative regimen doses are considered, D_{fixed}=75 mg and $D(\tau_1)$=75 mg. Dashed line indicates the limit of viral detection.

Firstly, analyzing the model without treatment, CD8+ T cells approach a level of 6.65×10^6 cells while viral load is undetectable about day 9. Using a curative regimen (75 mg dose), twice per day, the level of CD8+ T cells reaches a level of 4.17×10^6 cells and viral load is undetectable around day 7.5. For the control-based therapy, with an initial dose of $D(\tau_1)$=75 mg, promotes CD8+ T cells to 3.52×10^6 cells as a maximum, driving the viral load to be undetectable at day 7. Moreover, the control-based therapy improves the virological efficacy index Ψ over FDA therapy from 71% to 76%.

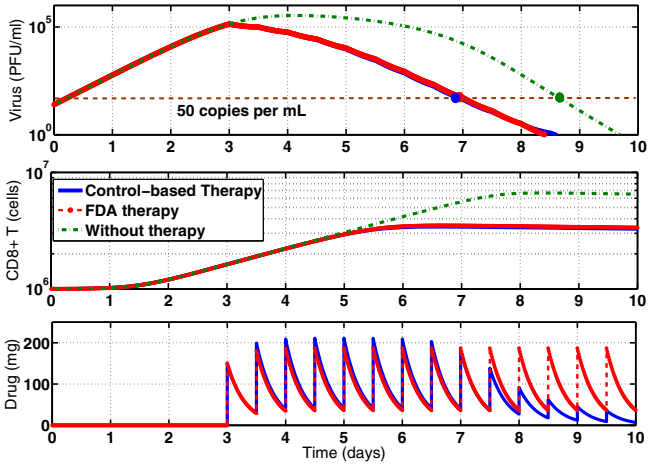

Fig. 3. Treatment strategies initiating at day 3. Pandemic regimen doses are considered, D_{fixed}=150 mg and $D(\tau_1)$=150 mg. Dashed line indicates the limit of viral detection.

For a pandemic regimen recommended by the FDA (D_{fixed}=150 mg) and an initial dose ($D(\tau_1)$=150 mg) for control-based, similar results occur as those in the curative regimen, see Fig. 3 and Table 3. Levels of CD8+ T cells are approximately 3.51×10^6 cells under FDA therapy while control-based therapy presents 3.41×10^6 CD8+ T cells. Over these therapies, both treatments make the viral load undetectable around day 7 as well as the virological efficacy index Ψ=79% for the two therapies.

Simulation results in Table 3 show that the curative regimen case and initial dose ($D(\tau_1)$=D_{fixed}=75 mg) for control-based, the amount of drug provided in the control-based therapy is larger than in FDA therapy (D_{fixed}) as well as the efficacy index Ψ. Also, viral clearance is observed earlier in the control-based strategy. However, for the pandemic regimen ($D(\tau_1)$=D_{fixed}=150 mg), the total amount of drug remains lower in the control-based therapy, that is 356 mg less for control-based therapy, while reaching the same efficacy index Ψ.

Table 3. Treatment initiation on day 3. Performance indices are presented for fixed dose (D_{fixed}) and control-based (CB).

	Amount of drug (mg)		**Index Ψ (%)**	
	D_{fixed}	CB	D_{fixed}	CB
75 mg	1050	1660	71	76
150 mg	2100	1744	79	79

4.2 Effects of Treatment Initiation

Drug efficacy is largely affected by treatment initiation time. To this end, we initiate treatment at day 2 and 4 separately. We keep using the two regimens, 75 mg and 150 mg, as tested in the previous subsection. Initiating at day 2, Fig. 4 shows the dynamics of the virus, CD8+ T

cells and drug dynamics. The number of CD8+ T cells, for FDA therapy is 3.48×10^6 and with control-based therapy is 2.56×10^6 cells. The virus is undetectable after day 7 with the control-based therapy while for the FDA therapy is almost at day 8. The respective efficacy indices are 96% for the control-based action and 93% for FDA therapy, both for the curative regimen.

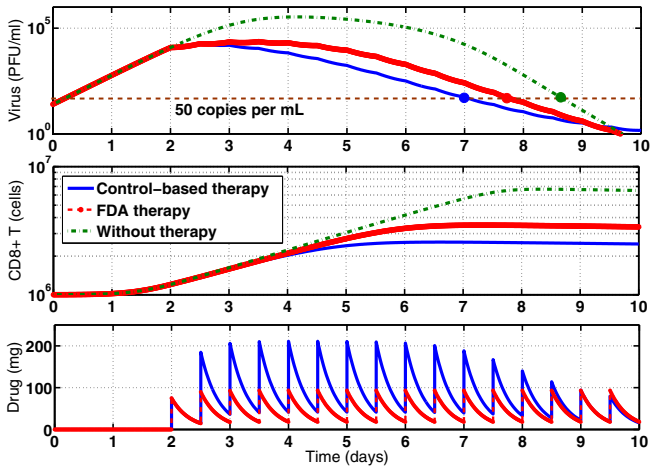

Fig. 4. Treatment strategies initiating at day 2. Curative regimen doses are considered, $D_{fixed} = 75$ mg and $D(\tau_1) = 75$ mg. Dashed line indicates the limit of viral detection.

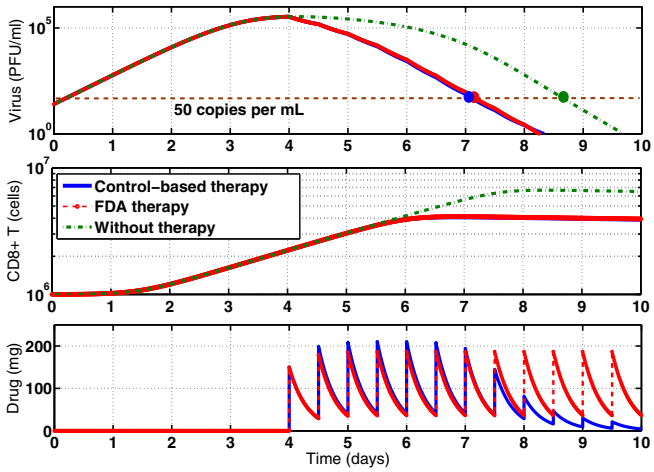

Fig. 5. Treatment strategies initiating at day 4. Pandemic regimen doses are considered, $D_{fixed} = 150$ mg and $D(\tau_1) = 150$ mg. Dashed line indicates the limit of viral detection.

Initiating at day 4, Fig. 5 shows the dynamics of the virus, CD8+ T cells and drug treatment. We observe that CD8+ T cells peaks at 4.11×10^6 cells for the FDA therapy and 4.03×10^6 for the control-based therapy. In both cases, the virus is undetectable after day 7. The efficacy index resulted in the same, 44% for both treatments in the pandemic regimen. In summary, initiating treatment at late phases of the infections, both strategies provide equivalent results.

Table 4. Treatment initiation on day 2. Performance indices are presented for fixed dose (D_{fixed}) and control-based (CB).

	Amount of drug (mg)		**Index Ψ (%)**	
	D_{fixed}	CB	D_{fixed}	CB
75 mg	1200	2194	93	96
150 mg	2400	2322	96	97

Table 5. Treatment initiation on day 4. Performance indices are presented for fixed dose (D_{fixed}) and control-based (CB).

	Amount of drug (mg)		**Index Ψ (%)**	
	D_{fixed}	CB	D_{fixed}	CB
75 mg	900	1303	38	41
150 mg	1800	1377	44	44

The amount of drug and virological efficacy index Ψ for doses of 75 and 150 mg are presented in Table 4 and Table 5. These tables present data for initiating treatment at day 2 and day 4 respectively. It is important to remark that in the case of treatment initiation at day 2, the control-based therapies presents slightly higher efficacy indices, over 95% of efficacy. Furthermore, the total amount of drug doses is slightly less for pandemic regimen cases of control-based therapy, compared with the amounts of FDA treatments with fixed doses. Initiating at day 4, the index Ψ is dropped to less than 50% of virological efficacy in all tests. In this sense, the 150 mg control-based therapy initiating at day 2 presents the best efficacy index Ψ. This highlights the relevance to initiate antiviral efficacy in the early phase of the infection, that is no after 2 days post infection.

5. CONCLUSIONS

This paper presents an integration of the IAV model to interact with the oseltamivir PK/PD dynamics, which resulted in a system that is represented as a semi-continuous impulsive system. Simulations show that initiating treatment at day 2, the control-based therapy reaches 96% and 97% of drug efficacy, over 93% and 96% of FDA treatment, for 75 and 150 mg of initial dose respectively. When treatment strategies are initiating 4 days post infection, both strategies provide poor viral efficacy. Further techniques that allow to schedule therapies at different time intervals will help us to advance steps towards clinical practices.

There are several aspects to improve in this work. First, observers design to viral infections as those presented in Alanis et al. (2014) can be pivotal to tackle the limited measurements in clinical practices. Moreover, bio-inspired optimization schemes can serve to optimal fine-tune control parameters presented in (18). Finally, advances in sub-optimal sampling schedules as in Cannon et al. (2016), can maximize information content of experimental outcomes for infection diseases, adding solutions to current limitations in clinical trials.

REFERENCES

Agoram, B.M., Martin, S.W., and van der Graaf, P.H. (2007). The role of mechanism-based pharmacokinetic–pharmacodynamic (PK–PD) modelling in translational research of biologics. *Drug discovery today*, 12(23), 1018–1024.

Alanis, A.Y., Hernandez-Gonzalez, M., and Hernandez-Vargas, E.A. (2014). Observers for biological systems. *Applied Soft Computing*, 24, 1175–1182.

Bakare, E.A., Nwagwo, A., and Danso-Addo, E. (2014). Optimal control analysis of an SIR epidemic model with constant recruitment. *International Journal of Applied Mathematical Research*, 3(3), 273–285.

Boianelli, A., Nguyen, V.K., Ebensen, T., Schulze, K., Wilk, E., Sharma, N., Stegemann-Koniszewski, S., Bruder, D., Toapanta, F.R., Guzmán, C.A., et al. (2015). Modeling influenza virus infection: A roadmap for influenza research. *Viruses*, 7(10), 5274–5304.

Boianelli, A., Sharma-Chawla, N., Bruder, D., and Hernandez-Vargas, E.A. (2016). Oseltamivir PK/PD modelling and simulation to evaluate treatment strategies against influenza-pneumococcus coinfection. *Frontiers in Cellular and Infection Microbiology*, 6, 60.

Canini, L., Conway, J.M., Perelson, A.S., and Carrat, F. (2014). Impact of different oseltamivir regimens on treating influenza A virus infection and resistance emergence: insights from a modelling study. *PLoS Comput Biol*, 10(4), e1003568.

Cannon, L., Garcia, C.A.V., Piovoso, M.J., and Zurakowski, R. (2016). Prospective HIV clinical trial comparison by expected kullback-leibler divergence. In *American Control Conference (ACC), 2016*, 1295–1300. IEEE.

Chandgude, N. and Pawar, S. (2016). Diagnosis of diabetes using fuzzy inference system. In *Computing Communication Control and automation (ICCUBEA), 2016 International Conference on*, 1–6. IEEE.

Chang, H., Moog, C.H., and Astolfi, A. (2012). A control systems approach to HIV prevention with impulsive control input. In *2012 IEEE 51st IEEE Conference on Decision and Control (CDC)*, 4912–4917. IEEE.

FDA (2008). Tamiflu (oseltamivir phosphate) capsules and for oral suspension. *Detailed view: safety labeling changes approved by FDA Center for Drug Evaluation and Research*, vol. 2008.

Gubareva, L.V., Kaiser, L., and Hayden, F.G. (2000). Influenza virus neuraminidase inhibitors. *The Lancet*, 355(9206), 827–835.

Haddad, W.M., Chellaboina, V., and Nersesov, S.G. (2006). *Impulsive and Hybrid Dynamical Systems: Stability, Dissipativity, and Control*. Princeton University Press.

Hernandez-Vargas, E.A., Colaneri, P., and Middleton, R.H. (2013). Optimal therapy scheduling for a simplified HIV infection model. *Automatica*, 49(9), 2874–2880.

Hernandez-Vargas, E.A., Middleton, R.H., and Colaneri, P. (2011). Optimal and MPC switching strategies for mitigating viral mutation and escape. *IFAC Proceedings Volumes*, 44(1), 14857–14862.

Hernandez-Vargas, E.A., Colaneri, P., and Middleton, R.H. (2014). Switching strategies to mitigate HIV mutation. *IEEE Transactions on Control Systems Technology*, 22(4), 1623–1628.

Imran, M., Malik, T., Ansari, A.R., and Khan, A. (2016). Mathematical analysis of swine influenza epidemic model with optimal control. *Japan Journal of Industrial and Applied Mathematics*, 33(1), 269–296.

Jaberi-Douraki, M. and Moghadas, S.M. (2014). Optimal control of vaccination dynamics during an influenza epidemic. *Mathematical biosciences and engineering: MBE*, 11(5), 1045–1063.

Lee, J., Kim, J., and Kwon, H.D. (2013). Optimal control of an influenza model with seasonal forcing and age-dependent transmission rates. *Journal of theoretical biology*, 317, 310–320.

Leon, B.S., Alanis, A.Y., Sanchez, E.N., Ornelas-Tellez, F., and Ruiz-Velazquez, E. (2013). Neural inverse optimal control applied to type 1 diabetes mellitus patients. *Analog Integrated Circuits and Signal Processing*, 76(3), 343–352.

Rivadeneira, P.S. and Moog, C.H. (2012). Impulsive control of single-input nonlinear systems with application to HIV dynamics. *Applied Mathematics and Computation*, 218(17), 8462–8474.

Rivadeneira, P.S., Moog, C.H., Stan, G.B., Brunet, C., Raffi, F., Ferré, V., Costanza, V., Mhawej, M.J., Biafore, F., Ouattara, D.A., et al. (2014). Mathematical modeling of HIV dynamics after antiretroviral therapy initiation: A review. *BioResearch open access*, 3(5), 233–241.

Rocha, D., Silva, C.J., and Torres, D.F. (2016). Stability and optimal control of a delayed HIV model. *Mathematical Methods in the Applied Sciences*.

Van der Graaf, P.H. and Benson, N. (2011). Systems pharmacology: bridging systems biology and pharmacokinetics-pharmacodynamics (PK-PD) in drug discovery and development. *Pharmaceutical research*, 28(7), 1460–1464.

Wattanagoon, Y., Stepniewska, K., Lindegårdh, N., Pukrittayakamee, S., Silachamroon, U., Piyaphanee, W., Singtoroj, T., Hanpithakpong, W., Davies, G., Tarning, J., et al. (2009). Pharmacokinetics of high-dose oseltamivir in healthy volunteers. *Antimicrobial agents and chemotherapy*, 53(3), 945–952.

WHO (2009). Guidelines for pharmacological management of pandemic influenza A(H1N1) 2009 and other influenza viruses. *World Health Organization*, vol. 20090820.

WHO (2014). World Health Organization, Influenza(seasonal) Fact sheet n. 211. *Fact sheet*, 211.

Yang, T. (1999). Impulsive control. *IEEE Transactions on Automatic Control*, 44(5), 1081–1083. doi: 10.1109/9.763234.